Physics and Imaging in Radiation Oncology 8 (2018) 38–43

Contents lists available at ScienceDirect

Physics and Imaging in Radiation Oncology

journal homepage: www.elsevier.com/locate/phro

Original Research Article

Design, fabrication, and validation of patient-specific electron tissue compensators for postmastectomy radiation therapy

Daniel F. Craft[a,b,*], Peter Balter[a,b], Wendy Woodward[b,c], Stephen F. Kry[a,b], Mohammad Salehpour[a,b], Rachel Ger[a,b], Mary Peters[a,b], Garrett Baltz[a,b], Erik Traneus[d], Rebecca M. Howell[a,b]

[a] Department of Radiation Physics, The University of Texas MD Anderson Cancer Center, Houston, TX 77030, USA
[b] The University of Texas Graduate School of Biomedical Sciences at Houston, Houston, TX 77030, USA
[c] Department of Radiation Oncology, The University of Texas MD Anderson Cancer Center, Houston, TX 77030, USA
[d] RaySearch Laboratories AB, Stockholm 111 34, Sweden

ARTICLE INFO

Keywords:
3D printing
Compensator
PMRT
Electrons

ABSTRACT

Background and purpose: Postmastectomy radiotherapy (PMRT) is complex to plan and deliver, but could be improved with 3D-printed, patient-specific electron tissue compensators. The purposes of this study were to develop an algorithm to design patient-specific compensators that achieve clinical goals, to 3D-print the planned compensators, and validate calculated dose distributions with film and thermoluminescent dosimeter (TLD) measurements in 3D-printed phantoms of PMRT patients.

Materials and methods: An iterative algorithm was developed to design compensators corresponding to single-field, single-energy electron plans for PMRT patients. The 3D-printable compensators were designed to fit into the electron aperture, with cerrobend poured around it. For a sample of eight patients, calculated dose distributions for compensator plans were compared with patients' (multi-field, multi-energy) clinical treatment plans. For all patients, dosimetric parameters were compared including clinical target volume (CTV), lung, and heart metrics. For validation, compensators were fabricated and irradiated for a set of six 3D-printed patient-specific phantoms. Dose distributions in the phantoms were measured with TLD and film. These measurements were compared with the treatment planning system calculated dose distributions.

Results: The compensator treatment plans achieved superior CTV coverage (97% vs 89% of the CTV receiving the prescription dose, $p < 0.0025$), and similar heart and lung doses ($p > 0.35$) to the conventional treatment plans. Average differences between calculated and measured TLD values were 2%, and average film profile differences were < 2 mm.

Conclusions: We developed a new compensator based treatment methodology for PMRT and demonstrated its validity and superiority to conventional multi-field plans through end-to-end testing.

1. Introduction

Post-mastectomy radiation therapy (PMRT) is the standard of care for node-positive breast cancer, because it has been shown to markedly reduce the risk of breast cancer recurrence and mortality [1]. However, planning and delivering PMRT is technically difficult. The desired radiation dose distribution should cover the chest wall and proximal lymph nodes but avoid the heart, lungs, and contralateral breast. Additionally, the chest wall thickness varies greatly, and large heterogeneities in tissue density must be accounted for in the treatment plan. Because of these difficulties, most PMRT plans involve multiple radiation fields that, despite being carefully matched, still result in hot and cold spots at field junctions [2].

Tissue compensators have been applied in PMRT as one approach to reducing treatment complexity, improving dose homogeneity, and eliminating hot and cold spots at field junctions [3–5]. Tissue compensators have also been used for similar purposes in a variety of disease settings, such as head and neck [6], soft tissue sarcomas [7], total body irradiation [8], and paraspinal muscle treatment [9]. Tissue compensators are versatile because they can even out almost any

* Corresponding author at: Department of Radiation Physics, The University of Texas MD Anderson Cancer Center, 1515 Holcombe Boulevard, Unit 94, Houston, TX 77030, USA.
E-mail address: rhowell@mdanderson.org (D.F. Craft).

https://doi.org/10.1016/j.phro.2018.11.005
Received 15 June 2018; Received in revised form 9 November 2018; Accepted 13 November 2018

surface, which makes simple, single-field treatments possible [10]. Despite the dosimetric advantages they provide, however, tissue compensators are not used frequently. Conventional techniques for compensator fabrication, such as wax molding and machine milling, are time-consuming and labor-intensive [10], and quality assurance of compensator devices is difficult. While there is a body of literature describing compensator design algorithms [11,12], these methods are generally not included as part of commercial treatment planning software.

Three dimensional (3D) printing technology has the potential to overcome the limitations of conventional fabrication techniques and reduce operational and production costs compared to conventional fabrication. 3D printers can be used to manufacture almost any arbitrary 3D volume by slicing that volume into layers and laying down one layer of solid material at a time. Fused deposition modeling (FDM) printers melt and extrude thermoplastics and then trace the extruder to fill the design for each layer, which can be as thin as 0.1 mm, allowing very fine printing resolution. These recent advancements in 3D printing require a reexamination of previously used techniques, and indeed there is a growing body of research showing interesting radiotherapy applications of 3D printing, including phantom production [13–17] and patient-specific devices [12,18–20], as well as extensive material analysis [12,21–23].

The purpose of this study was to prove the clinical feasibility of using 3D printed patient-specific compensators to improve and simplify PMRT relative to conventional 3D based photon plans with multiple energies and fields. Our aims were to 1) develop an algorithm within our commercial TPS to calculate compensator shapes and export them for 3D printing, 2) compare dose distributions from compensator based plans and clinical plans for actual patients with varying BMIs, and 3) validate calculated dose distributions with physical measurements by delivering compensator based plans to patient-specific phantoms.

2. Materials and methods

2.1. Algorithm design

We designed an iterative, four step algorithm (Fig. 1) to calculate patient-specific compensators. Between each step the user has opportunities to change settings or stop the script altogether. All but the end of step four are implemented as an internal script we wrote in RayStation 6R (RaySearch Laboratories, Stockholm, Sweden), which is a research version of the commercial TPS used in our clinic. This version of Raystation was specially modified to allow dose calculation with a compensator in the electron tray. All dose calculations were performed using Raystation's electron Monte Carlo algorithm.

Before starting the script a CTV must be defined. Once started, step one of the script will automatically create a new plan and add an electron beam, and then ask the user to set an appropriate *en face* gantry angle and isocenter position. Next, the algorithm automatically creates ROIs designating the cerrobend block and an initial, thin, flat compensator within the tray. Finally, an initial dose distribution is calculated, and the algorithm progresses to step two.

Step two of the algorithm modulates the shape of the compensator according to the previously calculated dose distribution. The difference between the actual, and prescribed dose is calculated at the distal edge of the CTV in a grid of user chosen size. Based on this dose difference, the anterior surface (that is, the target side) of the compensator is modulated along the ray line projected to that point. If the dose at the deep edge of the CTV is too high, the compensator thickness is increased, and if it is too low, the compensator thickness is decreased (with a minimum thickness of 1 mm). Once all grid points have been evaluated and the compensator shape modulated accordingly, a smoothing function is applied to reduce sharp edges.

Step three recalculates the dose in the patient using the newly modulated compensator shape from step two. At this point the script pauses, allowing the user to evaluate how well the plan meets clinical goals such as target coverage, lung dose, heart dose, skin dose, and more. If necessary, the user may change the electron energy or any other setting. If any settings are changed or if clinical goals are not met, the algorithm will go back to step two, then return to step three. This iterative process continues until the user is satisfied with the treatment plan.

Once the treatment plan is approved, the patient's ROI structures are exported and the compensator ROI is converted into a 3D model (with no smoothing) using the open-source DICOM image processing software 3DSlicerRT (Version 4.6, http://www.slicer.org) [24]. Finally, the 3D compensator model is turned into a 3D printable .gcode file using the 3D slicing software Simplify3D (Simplify3D; Cincinnati, OH). Printer settings are provided in Section 2.4.

2.2. Patient dose comparisons

Compensator plans were compared with conventional multi-field, multi-energy 3D plans for a sample of PMRT patients previously treated at our institution. As part of an Institutional Review Board approved protocol, we selected eight patients consecutively from a population of patients treated by the American Board of Radiology (ABR)–certified collaborating radiation oncologist (WW) between 12/1/2014 and 12/1/2015. The patients all had left-sided disease, were treated with deep inspiration breath hold, and are representative of the body mass index range in our clinic. All of the patients were treated with mixed energy (both 6 MV and 18 MV) photon opposed tangents and field-in-field modulation. Additionally, all patients' internal mammary nodes were treated with 1–2 electron beams of varying energy (4–16 MeV). The prescription for all patients was 50 Gy.

For each patient's standard of care treatment plan various dose metrics were recorded, including CTV coverage, heart dose, ipsilateral and total lung dose, extent of hot spots, skin dose, and CTV heterogeneity index. Heterogeneity index is defined according to Equation (1) [25].

$$HI = 100 * \frac{D_2 - D_{98}}{D_p} \quad (1)$$

D2, D98, and Dp stand for the minimum dose in 2% of the CTV (essentially the maximum CTV dose), minimum dose in 98% of the CTV (essentially the minimum CTV dose), and the prescription dose, respectively.

A new plan was then created for each patient using the algorithm described above, and the same dose statistics were recorded. Differences between each dose metric were tested for statistical significance using paired t-tests with an applied Bonferroni correction.

2.3. Film profile measurements

Due to the relatively rapid dose fall off in the distal edge of electron beams, we wanted to ensure we could accurately model the dose profile in patients when using compensator devices. To do this we designed a simple wedge shaped compensator in the TPS, printed it in polylactic acid (PLA), poured cerrobend around it to affix it in the electron tray, and measured dose profiles in solid water using EBT3 GAFchromic (Ashland, Bridgewater, NJ) film. We calibrated our film response using a 16 MeV electron beam in standard output check conditions. Film profiles were measured by placing film in line with the electron beam, surrounded by solid water. Five total sheets were irradiated; one at 12 MeV, three at 16 MeV, and one at 20 MeV. Measured and calculated film dose profiles were compared in four ways: depth of the central 80% isodose line, width of the 80% isodose line, and depth of the 80% isodse line 2 cm to the left and to the right of the central line.

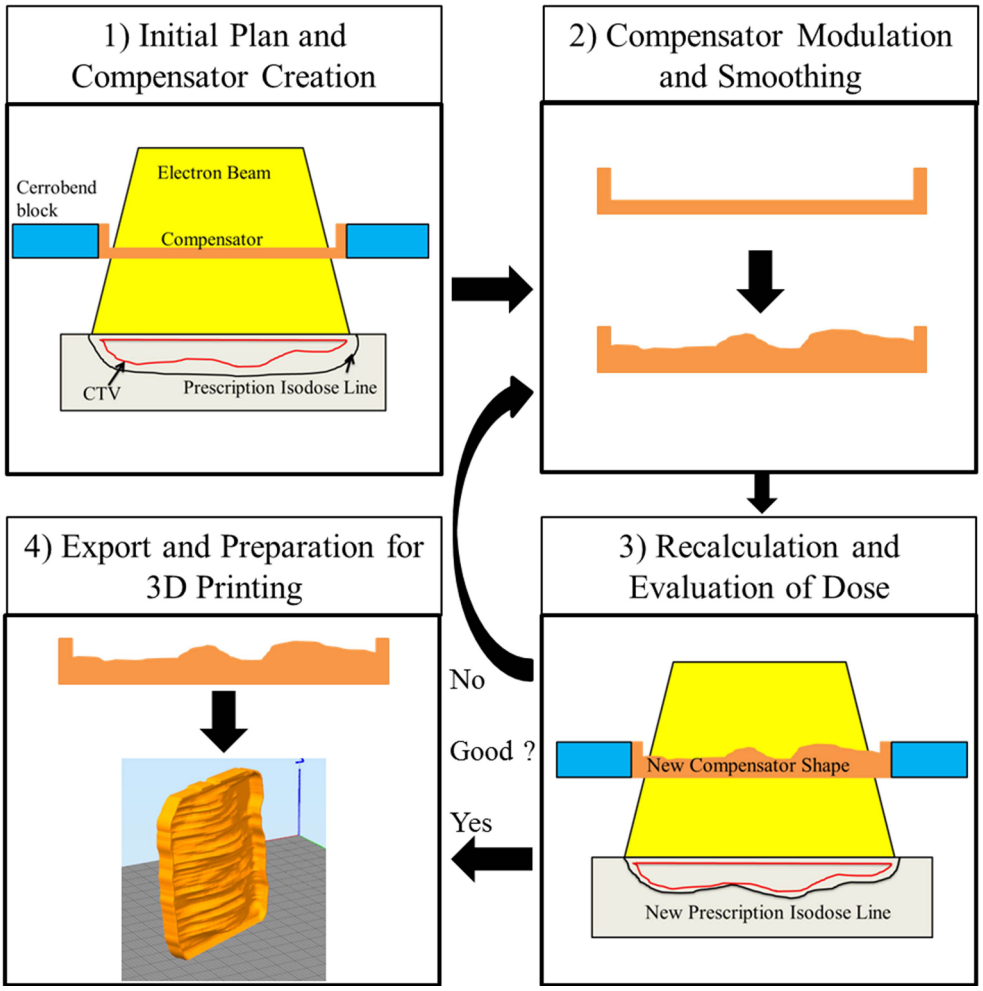

Fig. 1. Algorithm and compensator planning flow diagram. The four steps of the algorithm are shown, as well as the progression from step one to step two, the iteration between step two and step three until satisfactory plan conditions are met, and the final export and printing of the compensator as shown in step four.

2.4. Phantom validation measurements

In order to validate the full complexity of patient-specific compensators we designed compensator plans and printed physical compensators for six patient-specific anthropomorphic phantoms. Two phantoms each were based on patients in BMI category 2 (normal weight), category 3 (overweight) and category 4 (obese). These phantoms were 3D printed using our previously developed methods [13], and were based on the same population of patients described earlier (Section 2.2). Completed phantoms ranged from 11 to 13 slices and had masses ranging from 12.5 to 19.0 kg. The average material cost per phantom was $650, and the average printing time per phantom was 344 h.

Both the phantoms and compensators were printed out of PLA, using a Gigabot 3.0 printer (re3D, Houston, TX). All devices were printed using a nozzle temperature of 220 °C, a bed temperature of 55 °C, a print rate of 60 mm/s, 90% infill, two external walls, and a 0.3 mm layer height. 3D printed compensators took 10–15 h to print, and material costs averaged $30. Completed phantoms and compensators were CT imaged to ensure there were no internal air gaps or printing defects.

Each phantom was designed with cylindrical holes to hold 17 TLD detectors: five in the contralateral breast, three in the heart, and nine throughout the CTV. An additional three TLD skin packs were placed in the surface of each phantom directly anterior to the CTV. For each phantom the compensator plan was delivered as designed by the previously described algorithm using a Varian TrueBeam linear accelerator (Varian Medical Systems, Inc., Palo Alto, CA), and the TLD were analyzed following the methodology described by Kirby et al. [26], having an uncertainty of < 2.3%. Dose was also recorded in the TPS for each TLD location in the phantom, and these calculated and measured values were compared to determine the ability of the TPS to accurately model dose in patients for compensator based PMRT plans. The final phantom doses were calculated with the measured physical density of the printed phantom corrected in the TPS, according to recommendations regarding 3D printed devices previously published by our group [21].

3. Results

3.1. Patient dose comparisons

Compared to the standard of care clinical plans, the compensator based plans on average had superior dose coverage of the CTV with reduced hot spots. Statistically significant ($p < 0.0025$) improvements were achieved for CTV coverage (97% for compensator plans vs. 89% for 3D plans), heterogeneity indices (35.9 for compensator plans vs. 56.4 for 3D plans), and reduced hot spots in the lungs (1.7% receiving 40 Gy for compensator plans vs. 13.3% for 3D plans). Full results are summarized in Table 1.

Fig. 2 shows all eight patients' dose volume histograms averaged together into two DVH plots comparing the conventional 3D plan and the compensator based plan. As can be seen in the figure, CTV coverage is improved, while high dose regions in the lungs and CTV are reduced.

Table 1
. Comparison of dose metrics between conventional 3D plans and compensator based plans.

Dose Metric	Average 3D Plan	Average Comp Plan	Average Difference (Comp-3D)	p-value
CTV D98	39.0 Gy	44. 6 Gy	5.6 Gy	< 0.001
CTV Mean Dose	52.3 Gy	53.1 Gy	0.7 Gy	> 0.1
CTV D2	67.2 Gy	62.5 Gy	−4.7 Gy	0.06
CTV V45 Gy	89.1%	97.1%	8.0%	< 0.001
Heart Mean Dose	2.8 Gy	3.0 Gy	1.6 Gy	> 0.1
Heart V30 Gy	0.01%	0.3%	0.3%	0.06
Ips. Lung D2	52.1 Gy	39.0 Gy	−13.1 Gy	< 0.001
Ips. Lung V20 Gy	30.6%	34.3%	3.7%	> 0.1
Ips. Lung V40 Gy	13.3%	1.7%	−11.6%	< 0.001
Total Lung Mean Dose	7.5 Gy	7.6 Gy	0.1 Gy	> 0.1
Skin Mean Dose	40.8 Gy	52.2 Gy	11.5 Gy	< 0.001
Skin D2	57.7 Gy	62.1 Gy	4.4 Gy	0.02
HI	56.4	35.9	−20.5	< 0.001
110% Hotspot Volume	257 cm^3	170 cm^3	−87 cm^3	0.08
130% Hotspot Volume	32 cm^3	5 cm^3	−27 cm^3	0.09
150% Hotspot Volume	8 cm^3	0 cm^3	−8 cm^3	> 0.1

3.2. Film profile measurements

The average absolute differences between film measurements and TPS calculations were < 2 mm for all energies examined, see Table 2.

3.3. Phantom validation measurements

Fig. 3 shows photographs of a phantom and compensator plan, and TLD results are summarized in Table 3. Average disagreement between TPS and TLD doses in the CTV was 2% (as calculated with TLD doses assumed to be correct), and measured TLD doses outside the treatment area (heart and contralateral breast) agreed with TPS calculations within 17% (which for the out-of-field doses corresponds with an average absolute error of 5.6 cGy). Skin TLD pack doses agreed with the TPS within 3%.

Table 2
Average differences between calculated and measured dose profiles in film.

Energy (MeV)	Average Error in 80% Isodose Width (mm)	Average Error in 80% Isodose Depth (mm)	Overall Average Error (mm)
12	2.2	0.8	1.1
16	1.9	2.0	2.0
20	1.5	2.1	2.0
Average	1.9	1.7	1.7

4. Discussion

In this study we developed an in-house algorithm scripted within a commercial TPS to design patient-specific, 3D printable compensators for PMRT. These compensators are unique in that they are designed to fit within a standard electron tray, meaning we can use fast-printing, rigid materials that won't come in contact with the patient surface. We additionally have validated the dosimetry of the algorithm and 3D printed materials using film measurements in solid water and TLD measurements in 3D printed, patient-specific phantoms. Our results show that using 3D printing to fabricate patient specific PMRT compensators is clinically feasible, and in many ways superior to conventional 3D based PMRT treatment planning.

There are several advantages to using 3D printed compensators for PMRT treatments over the conventional plans the patients in this study previously received. In our treatment planning studies our compensator based plans show improved target coverage with the prescription dose, and reduced hot spots throughout the patient volume. While slightly more of the ipsilateral lung receives low dose than in conventional plans, our compensator plans dramatically reduce the high dose coverage in the lung (Fig. 2) because there are no tangent fields passing through the lung volume. Additionally, while the heart dose is elevated, the difference is not statistically significant and the doses are below all plan constraints for all cases. One dosimetric disadvantage of using these compensators is the elevated skin dose relative to conventional plans, which is not always desirable. This can be reduced by increasing the distance between the compensator and the skin, but this also negatively affects most other dose metrics.

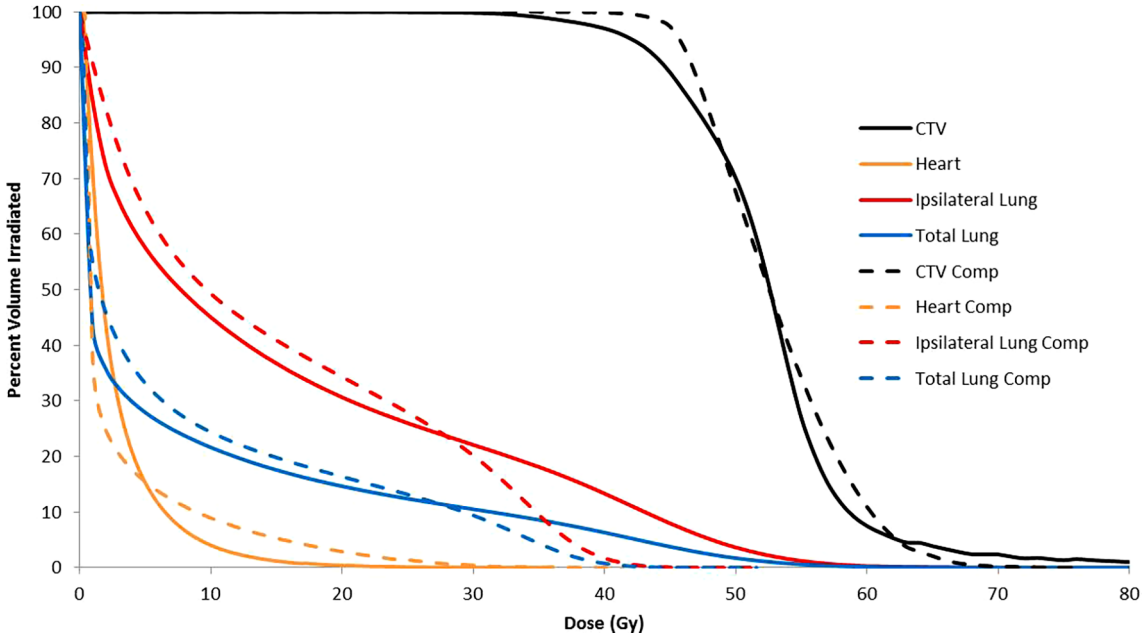

Fig. 2. Cumulative DVH comparison. The average of all compensator plan DVHs are shown with dotted lines, while the average of all conventional plans are shown as solid lines.

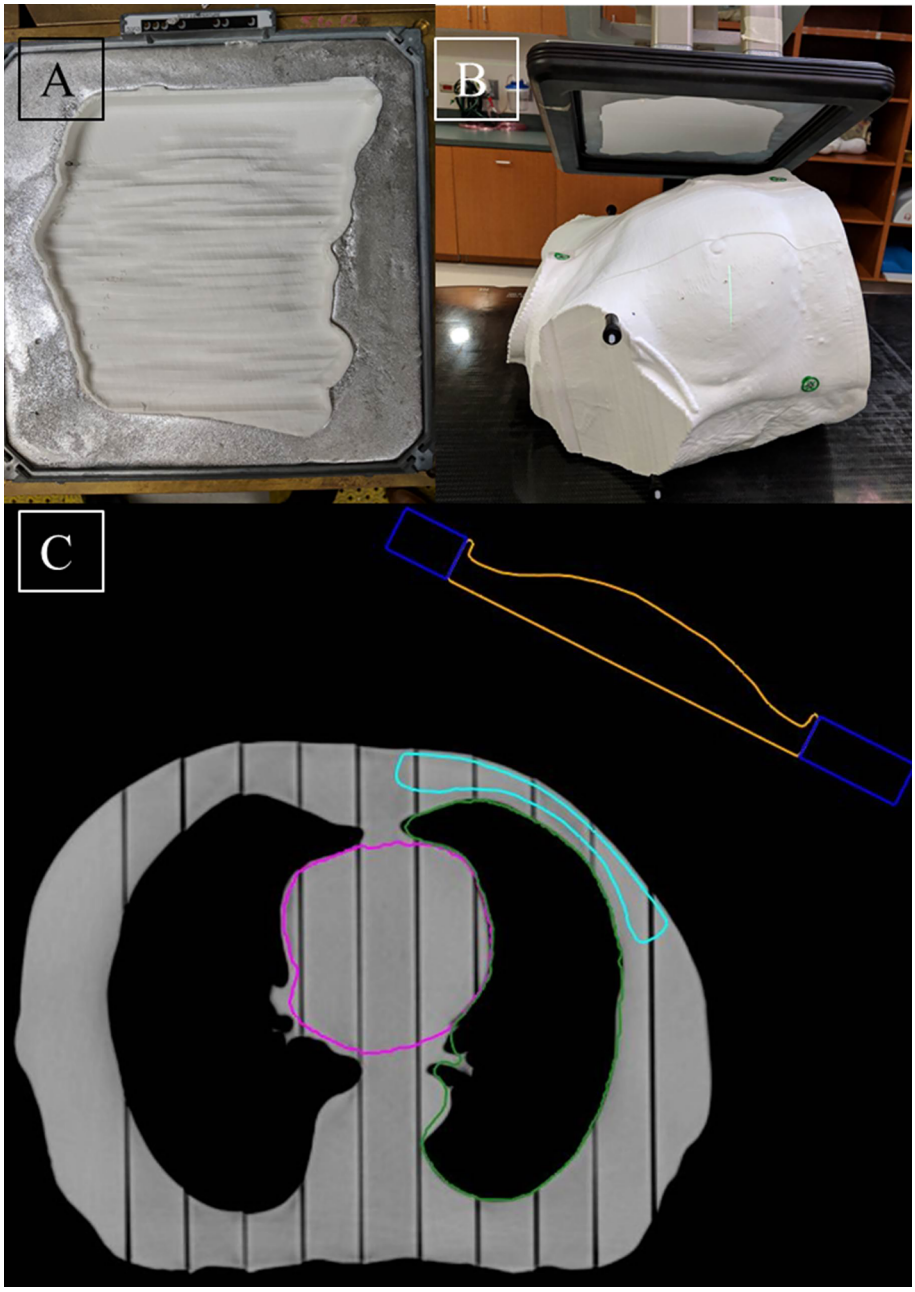

Fig. 3. Compensator plan delivery to a phantom. A) Photograph of the compensator in the cerrobend tray. B) Photograph of the compensator and phantom in treatment position, and C) Slice of the TPS view of the plan. In (C) the compensator is contoured in orange, the cerrobend in dark blue, the CTV in light blue, and the heart in pink. (For interpretation of the references to colour in this figure legend, the reader is referred to the web version of this article.)

Table 3
Summary of TLD dose calculation and measurement error.

Phantom	Average In-field TLD Error	In-field TLD Error SD	Average Out-of-field TLD Error	Out-of-field Error SD	Average Skin TLD Error	Skin Error SD
1	1%	1%	16%	9%	NA	NA
2	3%	1%	10%	7%	2%	1%
3	2%	1%	25%	25%	5%	2%
4	2%	1%	20%	12%	3%	1%
5	4%	2%	24%	17%	4%	1%
6	2%	2%	7%	9%	2%	2%
Average	2%	2%	17%	13%	3%	1%

Beyond dosimetric considerations, compensator plans are easier to set up and align than conventional multi-field plans due to the fact that there is only one field and one energy. With further testing the true extent of time saving will be elucidated, but in our experience we were able to set up and deliver a plan to a phantom on average every 15 min compared to the standard 30 min scheduled for PMRT patients at our clinic currently.

Another important aspect of this study was the use of 3D printed phantoms to validate dose calculations using complex, 3D printed, patient-specific compensators. These phantoms allowed us to accurately reflect the complex anatomy that exists in PMRT treatments, and to fully validate the accuracy of our treatment plans. Specifically, our film errors (2 mm), in-field TLD errors (2%), and skin TLD errors (3%) all showed high agreement with TPS calculations. Our out-of-field TLD agreed within 17% ± 13%, which is acceptable uncertainty compared

to other treatment planning systems and disease sites for out-of-field dose [27,28].

While many advantages exist for 3D printed compensators, there are also some disadvantages to our system. 3D printing is relatively inexpensive and straightforward, but does require some level of expertise and investment in resources. Additionally, much care must be taken to make sure that the unique composition of 3D printed materials is accounted for with density corrections in the TPS. Depending on the printing technique used, many standard materials, including PLA, may not fall on the standard CT calibration curve [21].

Another consideration is that not all PMRT patients can be adequately treated using this technique. For one of the patients in our study we were unable to meet our ipsilateral lung dose constraints due to the extreme thinness of the chest wall, and the large curvature of the full target area. For this patient the use of bolus in conjunction with the compensator could have improved the dose distribution, but to keep the comparison with other patients identical this was not attempted. For all other patients in our study we were able to meet all constraints. Additionally, the general methodology and underlying principles of our algorithm could be easily adapted to multiple other superficial treatment sites such as the head and neck, scalp, and extremities, potentially opening up 3D printed based compensator treatments to a much larger population of patients.

In conclusion, our results show the clinical feasibility of using patient specific 3D printed compensators for PMRT. Specifically, we were able to demonstrate statistically significant improved CTV coverage and reduced hot spots, as well as a simplified planning and delivery. Additionally, we found that we could accurately calculate dose in our TPS using custom compensators, with all in-field TLD errors < 3%. Additional work must be done to establish a clear patient workflow and QA procedure, but our results prove that 3D printed compensators are a clinically acceptable option for PMRT.

Disclosure of conflicts of interest

Erik Traneus works at RaySearch Laboratories.

Conflict of interest

None.

Appendix A. Supplementary data

Supplementary data to this article can be found online at https://doi.org/10.1016/j.phro.2018.11.005.

References

[1] McGale P, Taylor C, Correa C, Cutter D, Duane F, Ewertz F, et al. Effect of radiotherapy after mastectomy and axillary surgery on 10-year recurrence and 20-year breast cancer mortality: meta-analysis of individual patient data for 8135 women in 22 randomised trials. Lancet 2014;383:2127–35.

[2] Pierce LJ, Butler JB, Martel MK, Normolle DP, Koelling T, Marsh RB, et al. Postmastectomy radiotherapy of the chest wall: dosimetric comparison of common techniques. Int J Radiat Oncol Biol Phys 2002;52:1220–30.

[3] Kudchadker RJ, Hogstrom KR, Garden AS, McNeese MD, Boyd RA, Antolak JA. Electron conformal radiotherapy using bolus and intensity modulation. Int J Radiat Oncol Biol Phys. 2002;53:1023–37.

[4] Perkins GH, McNeese MD, Antolak JA, Buchholz TA, Strom EA, Hogstrom KR. A custom three-dimensional electron bolus technique for optimization of post-mastectomy irradiation. Int J Radiat Oncol Biol Phys. 2001;51:1142–51.

[5] Chang SX, Cullip TJ, Deschesne KM, Miller EP, Rosenman JG. Compensators: An alternative IMRT delivery technique. J Appl Clin Med Phys 2004;5:15–36.

[6] Kudchadker RJ, Antolak JA, Morrison WH, Wong PF, Hogstrom KR. Utilization of custom electron bolus in head and neck radiotherapy. J Appl Clin Med Phys 2003;4:321–33.

[7] Hong L, Alektiar KM, Hunt M, Venkatraman E, Leibel SA. Intensity-modulated radiotherapy for soft tissue sarcoma of the thigh. Int J Radiat Oncol Biol Phys 2004;59:752–9.

[8] Galvin JM, D'Angio GJ, Walsh G. Use of Tissue Compensators to Improve the Dose Uniformity for Total-Body Irradiation. Int J Radiat Oncol Biol Phys 1980;6:767–71.

[9] Low DA, Starkschall G, Sherman NE, Bujnowski SW, Ewton JR, Hogstrom KR. Computer-aided design and fabrication of an electron bolus for treatment of the paraspinal muscles. Int J Radiat Oncol Biol Phys 1995;33:1127–38.

[10] Williams PC. IMRT: delivery techniques and quality assurance. Br J Radiol 2003;76:766–76.

[11] Low DA, Starkschall G, Bujnowski SW, Wang LL, Hogstrom KR. Electron bolus design for radiotherapy treatment planning: bolus design algorithms. Med Phys 1991;19:115–25.

[12] Su S, Moran K, Robar JL. Design and production of 3D printed bolus for electron radiation therapy. J Appl Clin Med Phys 2014;15:194–211.

[13] Craft DF, Howell RM. Preparation and fabrication of a full-scale, sagittal-sliced, 3D-printed, patient-specific radiotherapy phantom. J Appl Clin Med Phys 2017;18:285–92.

[14] Gear JI, Long C, Rushforth D, Chittenden SJ, Cummings C, Flux GD. Development of patient-specific molecular imaging phantoms using a 3D printer. Med Phys 2014;41:0825021–825023.

[15] Gear JI, Cummings C, Craig AJ, Divoli A, Long CD, Tapner M, et al. Abdo-Man: a 3D-printed anthropomorphic phantom for validating quantitative SIRT. EJNMMI Phys 2016;3:17–32.

[16] Madamesila J, McGeachy P, Villarreal-Barajas JE, Khan R. Characterizing 3D printing in the fabrication of variable density phantoms for quality assurance of radiotherapy. Phys Med 2016;32:242–7.

[17] Ehler ED, Barney BM, Higgins PD, Dusenbery KE. Patient specific 3D printed phantom for IMRT quality assurance. Phys Med Biol 2014;59:5763–73.

[18] Sethi R, Cunha A, Mellis K, Siauw T, Diederich C, Pouliot J, et al. Clinical applications of custom-made vaginal cylinders constructed using three-dimensional printing technology. J Contemp Brachyther 2016;8:208–14.

[19] Ju SG, Kim MK, Hong CS, Kim JS, Han Y, Choi DH, et al. New technique for developing a proton range compensator with use of a 3-dimensional printer. Int J Radiat Oncol Biol Phys 2014;88:453–8.

[20] Burleson S, Baker J, Hsia AT, Xu Z. Use of 3D printers to create a patient-specific 3D bolus for external beam therapy. J Appl Clin Med Phys 2015;16:166–78.

[21] Craft DF, Kry SF, Balter P, Salehpour M, Woodward W, Howell RM. material matters: analysis of density uncertainty in 3D printing and its consequences for radiation oncology. Med Phys 2018;45:1614–21.

[22] Cunha A, Mellis K, Sethi R, Siauw T, Sudhyadhom A, Garg A, et al. Evaluation of PC-ISO for customized, 3D printed, gynecologic 192-Ir HDR brachytherapy applicators. J Appl Clin Med Phys 2014;16:246–53.

[23] Dancewicz OL, Sylvander SR, Markwell TS, Crowe SB, Trapp JV. Radiological properties of 3D printed materials in kilovoltage and megavoltage photon beams. Phys Med 2017;38:111–8.

[24] Fedorov A, Beichel R, Kalpathy-Cramer J, Finet J, Fillion-Robin JC, Pujol S, et al. 3D Slicer as an Image Computing Platform for the Quantitative Imaging Network. Magn Reson Imaging 2012;9:1323–41.

[25] Kataria T, Sharma K, Subramani V, Karrthick KP, Bisht SS. Homogeneity index: an objective tool for assessment of conformal radiation treatments. J Med Phys 2012;37:207–13.

[26] Kirby TH, Hanson WF, Johnston DA. Uncertainty analysis of absorbed dose calculations from thermoluminescence dosimeters. Med Phys 1992;19:1427–33.

[27] Huang JY, Followill DS, Wang XA, Kry SF. Accuracy and sources of error of out-of field dose calculations by a commercial treatment planning system for intensity-modulated radiation therapy treatments. J Appl Clin Med Phys 2013;14:186–97.

[28] Howell RM, Scarboro SB, Taddei PJ, Krishnan S, Kry SF, Newhouser WD. Methodology for determining doses to in-field, out-of-field and partially in-field organs for late effects studies in photon radiotherapy. Phys Med Biol 2010;55:7009–23.